Design of rough microgeometries for numerical simulation of material appearance

Benjamin Bringier, M Ribardière, Daniel Meneveaux, Lionel Simonot

Design of rough microgeometries for numerical simulation of material appearance

BENJAMIN BRINGIER[1,*], MICKAËL RIBARDIÈRE[1], DANIEL MENEVEAUX[1], AND LIONEL SIMONOT[2]

[1] University of Poitiers CNRS, XLIM, UMR 7252, France
[2] University of Poitiers CNRS UPR 3346 Institut Prime, France
[*] Corresponding author: benjamin.bringier@univ-poitiers.fr

Compiled April 15, 2020

Microfacet based material appearance models are commonly considered as a physical plausible representation of matter-light interaction. With such models, the microgeometry of a surface element is defined by a statistical distribution of microfacets. The mathematical formulation ensures physical plausibility, such as energy conservation and reciprocity. Many authors have addressed microfacet BSDF representations, with various Normal Distribution Functions (NDFs) and their relationship with shadowing and masking, or the effects due to multiple light scattering on the microgeometry. However, an extensive study on how an actual microgeometry drives material appearance still is missing. This question is a key issue for inverse design and manufacturing. This paper contributes in filling this gap by proposing a complete pipeline composed of a microgeometry generation process and numerical lighting simulation. From any input NDF, our method generates a controlled and structured microgeometry, integrated within numerical light scattering simulation. Reflected light is gathered using a virtual goniophotometer. From a given set of parameters, we use our pipeline to study the impact of microgeometry structures on material light scattering in case of rough surfaces. The obtained results are discussed and compared with already existing approaches when they exist in the pipeline.

http://dx.doi.org/10.1364/ao.XX.XXXXXX

1. INTRODUCTION

Though material appearance modeling has been studied for long, it still remains an intensive field of research. One key challenge is the prediction of reflectance using numerical simulation, in order to control or simulate the final aspect of a manufactured object [1]. In many cases, the mathematical models dedicated to material appearance (denoted as Bidirectional Scattering Distribution Function, or BSDF) must fulfill various requirements: Physical plausibility, ability to naturally represent existing/measured materials, visual realism, computation efficiency, etc. Microfacet distributions are considered nowadays as a reference for physically plausible BSDF representations and is widely studied for inverse design for instance.

With microfacet based BSDFs, a surface element is considered as a distribution of submillimeter facets, defined using a normal distribution function (or NDF). The steeper the slopes, the rougher the surface. In addition, shadowing and masking effects have to be accurately managed. Historically, this has been addressed using either two dimensional V-cavity profiles, or Smith's assumptions. The former is mathematically correct but does not correspond to realistic surfaces. The latter makes the assumption that microfacet normals (slopes) are not correlated, even in close proximity. Using one or the other model makes a visible difference on material appearance, especially for high roughnesses.

More recently, some authors have proposed using explicit microgeometry instead of a statistical representation. Light transfer is performed through path tracing simulation on the corresponding heightfield [2–4]. From a given normal distribution, multiple instances of microgeometry maps can be generated. For a given slopes distribution, strong disparities can appear, with varying structures, including deep valleys and large plateaus or high frequency surface variations. Besides, even small variations on the geometry may lead to quite different BSDFs.

To the best of our, no study has been proposed for the analysis of such variations in terms of surface versus BSDF, based on normal distributions. This paper proposes (i) a framework dedicated to the study of BSDF behavior, based on microfacet surface generation and (ii) an analysis of the variety of BSDFs produced depending on the surface roughness.

Based on normal distributions and their associated plausible microgeometries, our study relies on numerical lighting simulations, from flat surfaces, or constrained by predefined macrostructures. This approach provides a mean to study separately the first bounce and the multi-bounce scattering effect.

Light scattered by the surface is gathered by a virtual goniophotometer, that mimics real devices. We show how material appearance changes (i.e. changes in the BSDF) according to the underlying microgeometry, and we study the impact of microgeometry divergences in the corresponding BSDF, especially for very rough surfaces. Our results illustrate various BSDFs obtained with various microgeometry structures, that can be employed for improving material appearance with inverse design processes. We discuss and compare our framework with several approaches used in the litterature, most of them employed in contexts different from ours: (i) surface reconstruction methods from normal distributions; (ii) estimation of multi-bounce light scattering in microfacet-based BSDFs.

This article is broken down into three distinct parts. The first one introduces the BSDF microfacet theory, and gives an overview of the proposed method, according to the state of the art. The second one shows the framework to construct a heightmap from a normal distribution function. The last part proposes a study on material appearance depending on the properties of the microgeometry, including the comparisons mentioned above.

2. BACKGROUND AND OVERVIEW

The Bidirectional Scattering Distribution Function (or BSDF) $f(\mathbf{i},\mathbf{o},\mathbf{n})$ describes how a surface element dS of normal $\mathbf{n}$ (lit by a collimated light source from direction $\mathbf{i}$) reflects light toward an observer direction $\mathbf{o}$. It is defined as the ratio between the radiance $L(\mathbf{i},\mathbf{o},\mathbf{n})$ reflected by dS toward $\mathbf{o}$, and the incident irradiance $E(\mathbf{i},\mathbf{n})$ coming from direction $\mathbf{i}$ (notations are presented in Figure 1).

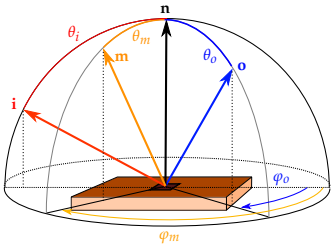

Fig. 1. Geometry of reflection and notations.

A BSDF model is considered as *physically plausible*, if it satisfies Helmoltz reciprocity $f(\mathbf{i},\mathbf{o},\mathbf{n})=f(\mathbf{o},\mathbf{i},\mathbf{n})$, and energy conservation $\int_{\Omega_+} f(\mathbf{i},\ \mathbf{o},\ \mathbf{n})\ |\mathbf{o}\cdot\mathbf{n}|\ d\omega_o\ \leq 1,\ \forall \mathbf{i}\in\Omega_+$.

The microfacet representation of a BSDF $f(\mathbf{i},\mathbf{o},\mathbf{n})$ is based on a statistical description of a microfacet distribution. The general equation is given by:

$$f(\mathbf{i},\mathbf{o},\mathbf{n}) = \int_{\Omega_+} \frac{|\mathbf{i}\cdot\mathbf{m}|}{|\mathbf{i}\cdot\mathbf{n}|} f^{\mu}(\mathbf{i},\mathbf{o},\mathbf{m}) \frac{|\mathbf{o}\cdot\mathbf{m}|}{|\mathbf{o}\cdot\mathbf{n}|} D(\mathbf{m}) G(\mathbf{i},\mathbf{o},\mathbf{m}) d\omega_m \quad (1)$$

where $f^{\mu}(\mathbf{i},\mathbf{o},\mathbf{m})$ is the BSDF of an individual microfacet associated with a normal $\mathbf{m}$. Its contribution is weighted by the distribution $D(\mathbf{m})$ and a geometric attenuation factor $G(\mathbf{i},\mathbf{o},\mathbf{m})$. $D(\mathbf{m})$ is the Normal Distribution Function (NDF) that defines the surface roughness, indicating the proportion of microfacets corresponding to a normal $\mathbf{m}$; $G(\mathbf{i},\mathbf{o},\mathbf{m})$ expresses the portion of a microfacet of normal $\mathbf{m}$ visible from both the light source and the observer. Many authors have studied the combinations of distributions and geometric attenuation factors [5–14], that have to be carefully chosen together [9, 15].

Microfacets are supposed to be oriented toward the upper hemisphere ($D(\mathbf{m})=0$ if $\mathbf{m}\cdot\mathbf{n}\leq 0$), and their projected areas have to be equal to the macroscopic surface:

$$\int_{\Omega_+} D(\mathbf{m})|\mathbf{m}\cdot\mathbf{n}|d\omega_m = 1.$$

This paper focuses on purely specular microfacets [5, 6, 11], for which Equation 1 simplifies to:

$$f(\mathbf{i},\mathbf{o},\mathbf{n}) = \frac{F(\mathbf{i},\mathbf{h})D(\mathbf{h})G(\mathbf{i},\mathbf{o},\mathbf{h})}{4|\mathbf{i}\cdot\mathbf{n}||\mathbf{o}\cdot\mathbf{n}|}, \quad (2)$$

where $\mathbf{h}=\frac{\mathbf{i}+\mathbf{o}}{||\mathbf{i}+\mathbf{o}||}$ is the half-angle vector between $\mathbf{i}$ and $\mathbf{o}$, and $F(\mathbf{i},\mathbf{h})$ corresponds to Fresnel's reflectance, depending on n_i, the relative refractive index between the material and the exterior medium refractive index.

Shadowing and Masking

The geometrical attenuation function $G(\mathbf{i},\mathbf{o},\mathbf{m})$ accounts for self-masking and self-shadowing. The widely used function proposed by Torrance and Sparrow [5] makes the assumption that the microsurface corresponds to a set of two dimensional V-cavity profiles. The shadowing/masking term is thus given by

$$G(\mathbf{i},\mathbf{o},\mathbf{h}) = \mathbf{max}\left[0, \mathbf{min}\left[1, \frac{2|\mathbf{i}\cdot\mathbf{n}||\mathbf{h}\cdot\mathbf{n}|}{|\mathbf{i}\cdot\mathbf{h}|}, \frac{2|\mathbf{o}\cdot\mathbf{n}||\mathbf{h}\cdot\mathbf{n}|}{|\mathbf{o}\cdot\mathbf{h}|}\right]\right]. \quad (3)$$

This model is mathematically consistent but physically unrealistic [15], since no real surface may correspond to the V-cavity assumption. Nowadays, it is widely agreed that Smith's shadowing-masking term [7, 16] is closest to the physical reflection behavior of rough surfaces. Shadowing and masking are considered as independent, and $G(\mathbf{i},\mathbf{o},\mathbf{m})$ is thus approximated using the product of the same two functions G_1:

$$G(\mathbf{i},\mathbf{o},\mathbf{m}) = G_1(\mathbf{i},\mathbf{m})\ G_1(\mathbf{o},\mathbf{m}). \quad (4)$$

The most important assumption in Smith's term is that microfacet normals are not correlated, even in close proximity. Mathematically, this assumption can be written as follows:

$$G_1(\mathbf{v},\mathbf{m}) = \begin{cases} G_1(\mathbf{v}) & \mathbf{v}\cdot\mathbf{m} \geqslant 0 \\ 0 & \mathbf{v}\cdot\mathbf{m} < 0 \end{cases} \quad (5)$$

It has been used by Ashikhmin et al. [9] to derive the following expression:

$$G_1(\mathbf{v}) = \frac{(\mathbf{v}\cdot\mathbf{n})}{\int_{\Omega_+(\mathbf{v})}(\mathbf{v}\cdot\mathbf{m})D(\mathbf{m})\ d\omega_m}. \quad (6)$$

More convenient expressions of this function can be obtained starting from the work proposed by Bourlier et al. [7]. For instance, Walter et al. [11] and more recently Heitz [15] have expressed the normal distribution in slopes space $P_{22}(p,q)$:

$$P_{22}(p,q) = \cos^4\theta_m\ D(\mathbf{m}), \quad (7)$$

where p and q correspond to the microsurface slopes in the macrosurface local coordinate system, defining the normal $\mathbf{m}$, such that $p^2+q^2=\tan^2\theta_m$. The one-dimensional distribution of slopes is given by:

$$P_2(q) = \int_{-\infty}^{+\infty} P_{22}(p,q)\ dp. \quad (8)$$

Finally, $G_1(\mathbf{v})$ is obtained by the integration of P_2:

$$G_1(\mathbf{v}) = \frac{1}{1+\Lambda(\mathbf{v})}, \tag{9}$$

where $\Lambda(\mathbf{v}) = \frac{1}{\mu}\int_{-\infty}^{+\infty}(q-\mu)P_2(q)\,dq$ and $\mu = \cot\theta_v$. A formal proof of these derivations is given by Heitz [15].

Ross et al. [17] or Heitz et al. [18] propose formulations with the assumption that masking and shadowing are correlated. These versions are considered as physically more plausible. The following expressions is considered by several authors as the most accurate for masking and shadowing, with an equivalent computational cost:

$$G(\mathbf{i},\mathbf{o},\mathbf{m}) = \frac{1}{1+\Lambda(\mathbf{i})+\Lambda(\mathbf{o})}. \tag{10}$$

Smith's shadowing-masking factor directly depends on the chosen NDF. This latter thus has to be carefully chosen in order to derive an analytical expression for G_1 (Equation 6) and Λ (Equations 9 or 10).

Study overview

Microfacet based BSDF formulation, as stated in Equations 1 and 2, suffers from two major limitations. The first one is inherent to its statistical background which does not correspond to actual microgeometry profiles. Both assumptions (V-cavity and Smith) consider that no correlation exist between microfacet slopes: This is often broken with real world materials, especially with manufactured objects. The second limitation is related to the fact that microfacet BSDF models do not take into account the scattering of light between microfacets. The lighting simulation process thus results in abnormally dark surfaces, due to incorrect loss of energy, even with non-absorptive materials. This is particularly true with highly rough surfaces associated with steep slopes microfacets: Microfacet models assume that light is not scattered and never leaves the surface. A recent work proposed by Heitz et al. [19] handles these effects with specific normal distributions (Beckmann [20] and GGX [11]). Kulla and Conty [21] or Turquin [22] propose to precompute and tabulate a non physically based approximation of the lost energy, according to the distribution roughness parameter for the same NDFs. Multiple scattering has also been recently addressed in the context of V-cavity profile assumptions [23–25]. All these methods are build upon a statistical representation of the surface associated to the corresponding assumptions,V-cavity or Smith, and not with actual microgeometry.

However, multiple microfacet geometric configurations may correspond to the same NDF. The way how the surface structures drive the optical behavior of the material is not addressed in microfacets based BSDF models and constitute one of their weaknesses.

One important issue addressed in this paper concerns the construction of a microfacet surface mesh from a slopes (or normal) distribution in order to estimate the actual observed BSDF, including light multiple scattering on the surface itself. The key issue is to construct a plausible surface from a given normal distribution. Many authors have proposed to generate heightfields from height probability distributions and autocorrelation [26, 27], but they cannot be extended to slope distributions [2]. C^0 continuous surface have been generated by several authors from Gaussian slope probability distributions [4], or continuous C^{-1} surface (i.e., with height discontinuities) from non-Gaussian slope probability distributions [28–30]. Weyrich et al. [31, 32] propose an approach suitable for non-Gaussian surfaces, but it still does not ensure surface continuity and it is not designed to reproduce smooth distributions [33].

Ribardière et al. [2] propose a framework for building explicit surfaces from any input NDF, and estimating BSDF. This paper extends this framework and studies the impact of microgeometry on material appearance for several configurations. As stated above, previous methods [19, 23, 24] represent multiple light interactions only through statistical representations of the surface: Either with V-cavities for [23, 24] (Figure 2-a), or with microflakes where microfacets never join in [19] (Figure 2-b). Neither of them corresponds to a possible realistic microgeometry. Instead, we propose to generate a microgeometry from any statistical description through the NDF (Section 3). We then run numerical lighting simulation, and a virtual goniophotometer gathers reflected light (Section 4-A). Our surface reconstruction procedure includes the management of topology constraints to control the microgeometry structure, and may use a user-defined input surface. A wide range of microgeometry shapes can be generated thanks to this process for one given NDF. Based on this framework we study the connections between microgeometry shapes and material appearance for rough microsurfaces.

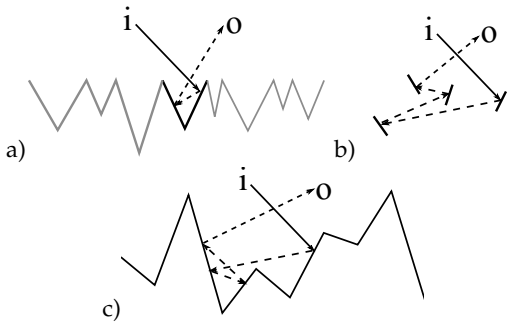

Fig. 2. Statistical methods (a-b) simulate light interaction with unrealistic microgeometry: (a) V-cavity profiles and (b) microflakes. (c) Our method allows to generate explicit microgeometry from any statistical description of the geometry (NDF) and performs numerical lighting simulation on this surface to compute the corresponding BSDF.

3. MICROSURFACE CONSTRUCTION

The goal of our method is to construct a surface from a set of $\mathfrak{L}_\mathbf{m}$ microfacet orientations, generated by an importance sampling process (based on the chosen distribution function, see Figure 3.a). In practice, the procedure consists in rearranging the normals on a uniform grid, so as to produce a C^0 continuous surface (i.e., without discontinuities). Unfortunately, for a grid size of 4096 by 4096 vertices, the number of possible permutations in $\mathfrak{L}_\mathbf{m}$ is $2^{24}!$. A brute-force algorithm is thus not suitable for exploring all the solutions. Instead, we propose to employ an iterative shape-from-gradient approach, suitable with any distribution: First, the set of normals $\mathfrak{L}_\mathbf{m}$ is randomly distributed on the regular grid. Second, a microfacet surface is produced thanks to this distribution, using integration, providing a starting surface. Unfortunately, the resulting slopes distribution is not consistent with the initial NDF. The iterative process consists in the following steps (see Figure 3): (b) The derivative is computed, in order to derive the associated gradient field ∇h^+; (c) The normals of the obtained surface are replaced by the closest

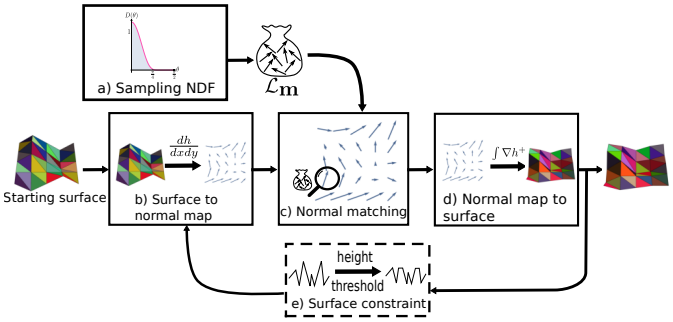

Fig. 3. Flow chart of surface reconstruction: From a sampling NDF (a), a normal map is generated with or without a starting surface; Then, an iterative process is used to converge towards a surface with the same NDF (b-d); Some constraints could be applied at each iteration (e).

possible normals in $\mathfrak{L}_\mathbf{m}$ (each normal in $\mathfrak{L}_\mathbf{m}$ is used only once), based on a random process in order to spread the matching error on the surface ; (d) The resulting normal map defines a new gradient field to integrate, producing a new rough surface h; This process is repeated from (b) to (d) until convergence.

This process ensures that the final surface is not spatially correlated. We propose to enrich the process with specific starting surfaces, chosen by the user, in order to introduce surface macro-structures. In addition, we have managed surface constraint filters (Figure 3.e), that can operate before the next iteration. As an example, we have employed height limitation.

Several methods have been proposed in the literature for integrating a noisy gradient field ∇h (i.e., with discontinuities) [34–36]. The conversion of ∇h into a height field h requires that ∇h complies with Schwarz's theorem, expressed in its discrete form as:

$$\frac{\partial h(x,y)}{\partial x} + \frac{\partial h(x+1,y)}{\partial y} = \frac{\partial h(x,y)}{\partial y} + \frac{\partial h(x,y+1)}{\partial x}. \quad \textbf{(11)}$$

We have chosen the Frankot-Chellappa algorithm [37], that relies on a Fourier transform applied to the gradient field. This solution guarantees Dirichlet boundary conditions, and the results are obtained within short computation times, even for large surfaces. It consists in minimizing a least square error function W defined by the following equation:

$$W = \int\int \left(\frac{-\partial h(x,y)}{\partial x} - p\right)^2 + \left(\frac{-\partial h(x,y)}{\partial y} - q\right)^2 dxdy, \quad \textbf{(12)}$$

where $h(x,y)$ is the original surface. Using Parseval's theorem, the expression that links the Fourier transform of the surface $H(u,v)$ and the Fourier transform $P(u,v)$ and $Q(u,v)$ of the gradients $\left\{p = \frac{\partial h}{\partial x}, q = \frac{\partial h}{\partial y}\right\}$ is:

$$H(u,v) = \frac{-juP(u,v) - jvQ(u,v)}{u^2+v^2}, \quad \textbf{(13)}$$

where $(u,v) \neq (0,0)$. From this relation, a surface h is directly obtained by the inverse Fourier transform of H. Due to the use of the fast Fourier transform, a surface is obtained from a gradient filed within short computation times, even for large surfaces.

In the same way, Step (c) is accelerated thanks an accelerating structure. The normals of $\mathfrak{L}_\mathbf{m}$ expressed in the gradient domain p and q, are placed in a uniform grid. The matching of $\nabla h^+(x,y)$ from unused values of $\mathfrak{L}_\mathbf{m}$ is then performed in a selected cell. In case of missing value, the search is performed in neighboring cells, using with a spiral path.

In the remainder of this paper, all the generated surfaces correspond to a grid of 4096 by 4096 pixels. According to the constraints defined at step (e) or to the starting surface, and from a given normal distribution, the proposed method may produce surfaces with very different properties in terms of macro-structure or height autocorrelation functions.

Figure 4 illustrates an example of four different surfaces obtained from GGX distribution with $\sigma = 1.0$ and various configurations of the proposed method. A height threshold $Zlim$ is used at step (e) (see Figure 4.b), is expressed in number of pixel. As illustrated in Figure 4, applying surface constraints does not alter the non-correlation property while allowing to change the macro-geometry appearance.

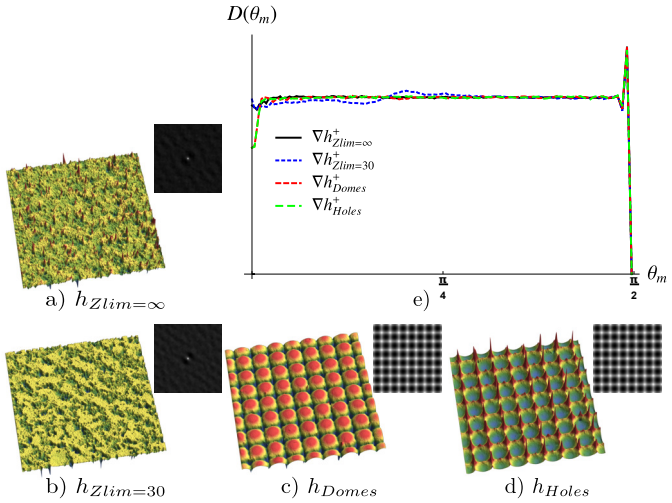

Fig. 4. Four height-maps obtained from GGX distribution, with $\sigma = 1.0$ and (a) a full random process, (b) no starting surface with an height control for the surface constraint step, (c-d) microfacets obtained with two different starting surfaces, respectively a "Domes" and a "Holes" surface (without any height constraint). For each result, the autocorrelation function is provided in inset and (e) final normal distribution.

The surfaces generated with this method follow the Smith's assumptions[16], unless a specific starting surface is employed; The latter defines the final autocorrelation function. This type of surface generally corresponds to manufactured objects. The four examples produced by our method finally have the same microfacet normal distribution. The estimated accuracy between desired and obtained normal distribution curves should take the projected microfacet area ($\sin\theta_m$) into account. For instance, with a given isotropic GGX distribution with $\sigma = 1.0$, the final surface will be defined using a low number of microfacets with a normal angle θ_m close to 0 and a high number of microfacets with a normal angle θ_m close to $\frac{\pi}{2}$.

4. LIGHT SCATTERING SIMULATION AND ANALYSIS

From a surface obtained using the reconstruction process described above[1], numerical lighting simulations can be performed, in order to gather the corresponding practical BSDF. Our virtual goniophotometer is described in Section A. In the

[1]Note that the obtained heighfield is converted to geometrical mesh composed of triangles

case of Beckmann's distribution, a comparison is given in Section B. The chosen case studies and the results of our analysis are discussed in Section C.

The panel of appearance configurations that can be produced by microfacet based BSDF is infinitely wide, and we propose to address the main features offered by our method for generating rough microgeometry and simulating the material appearance. Moreover, for the sake of clarity, we set the Fresnel term to 1, that corresponds to perfect mirror microfacets, and we consider a mono-wave length case.

A. Virtual Goniophotometer

Let us consider a virtual gonioreflectometer defined as a hemispherical sensor [38] with equal-area cells (i.e., iso-solid angle and with the same aspect ratio for all cells to mitigate acquisition bias). Similarly to a real gonioreflectometer system, a collimated light beam illuminates the microsurface from a fixed direction, defined by spherical angles θ_i and φ_i (Figure 5).

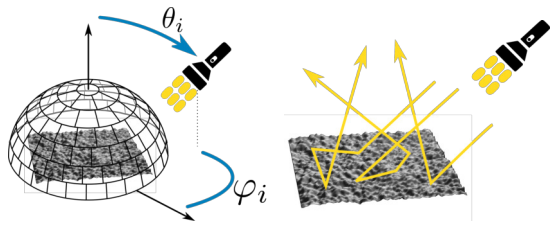

(a) Hemispherical sensor **(b)** Numerical lighting simulation

Fig. 5. Virtual goniophometer and lighting simulation

The reflected light leaving the microsurface is captured by the hemispherical sensor cells, after one bounce (L_1), two bounces (L_2), or more (L_{2+}). The resulting histogram (i.e., values gathered in each sensor's cell) is proportional to $f(\mathbf{i},\mathbf{o})\cos\theta_o$, with $\mathbf{o}$ the center direction of one sensor's cell. Virtual gonioreflectometers have been used for long [39, 40] and by many authors. Our system differs from these previous work in two ways: (i) It handles all light bounces on the surface, and (ii) it uses a high resolution sensor instead of basis functions (e.g. spherical harmonics in [39, 40]), that are prone to filtering artifacts and/or require a large number of coefficients. In our case, the maximum area of the sensor cells have to be carefully chosen, because accuracy depends on (i) the generated surface size and (ii) the input normal distribution roughness. We generate 4096^2 grids, corresponding to $16mm^2$ real patches. To efficiently cover all the surface, the number of light paths samples for each incident direction is set to 3×4096^2. The goal is to statistically reach all the sensor cells. The angular cell resolution is set to 0.35°, for all the results produced in this paper. It corresponds to a balance between avoiding over-filtering effects due to low number of cells, and noisy representation in reconstructed signal due to too small cells (Figure 6). As a comparison, the EZ-Contrast from Eldim [41] has an angular resolution of 0.4° and the ConDOR facility (Conoscopic Device for Optic Reflectometry) [42] developed by the LNE-CNAM has an angular resolution of 0.018° (this is one of the most precise existing device). The latter is dedicated to study the shape of a 1° width specular peak that does not correspond to our level of surface roughness study. With this system, only the specular peak can be analyzed, because of the required acquisition time.

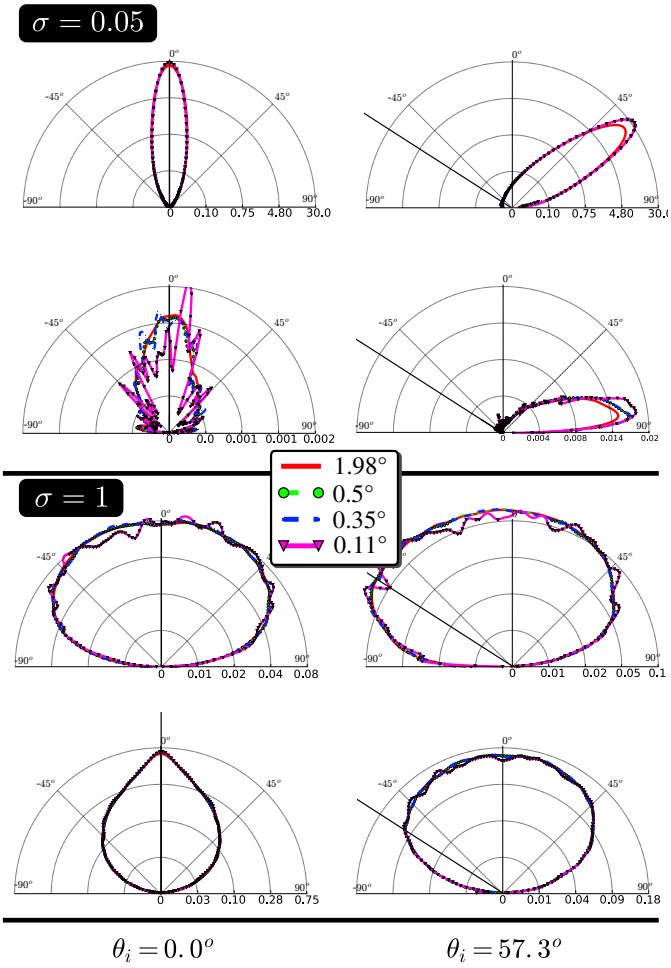

Fig. 6. Sensor resolution has to be carefully chosen according to the BSDF signal reconstruction accuracy. Low resolutions produce strong filtering effects while high resolutions produce noisy signals. The virtual goniophotometer is employed with 4096^2 2D mesh grids, built from GGX distribution with $\sigma = 0.05$ (high frequency BSDF) and $\sigma = 1$ (low frequency BSDF). For each roughness, first row stands for L_1 and second row for L_{2+}.

B. Comparisons with existing approaches

Firstly, we propose a comparison of our microsurface construction against the method proposed by Heitz et al. [3, 4]. This latter is limited to Beckmann's distribution, and to the best of our knowledge no other alternative exists in the literature for generating a C_0 continuous surface from a given normal distribution. As shown in Figure 7, the results are similar for both L_1 (with height correlated Smith's GAF) and L_{2+}. This results illustrates that for the specific case of Beckmann's distribution, our approach provides consistent results compared to Heitz's.

Secondly, we also provide comparisons of light multiple reflexions on microfacet surfaces with the two most recent approaches: (i) V-cavity representations, that received recent improvement to take into account multiple-scattering [23, 24]; (ii) Heitz's approach [19], based on a fully probabilistic raytracing built upon Smith's assumptions [16]. Figure 8 illustrates the results of BSDF simulations corresponding to GGX distribution with $\sigma = 1.0$ for both L_1 and L_{2+} and for two incident directions ($\theta_i = 0^o$ and $\theta_i = 57.3^o$). BSDF values are represented

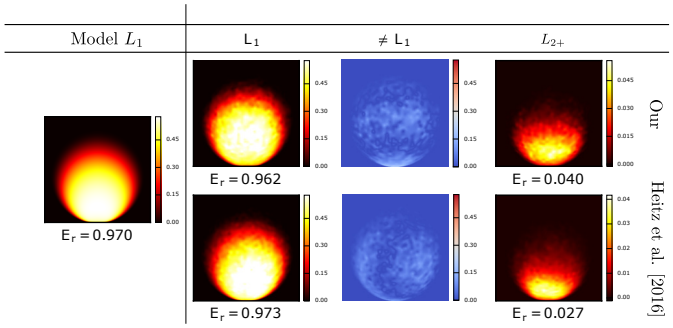

Fig. 7. BSDF comparisons with Beckmann's distribution ($\sigma = 0.75$), between surfaces generated with Heitz's method [3] and ours. The incident angle is $\theta_i = 1.5$ rad, with E_r the total amount of reflected energy, L_1 one-bounce BSDF, and L_{2+} multiple-bounce BSDF only. Column *Model* L_1 corresponds to Cook-Torrance model (one bounce only), Column $\neq L_1$ corresponds to the absolute difference between L_1 and *Model* L_1.

in false color with a projection of the virtual goniophotometer hemispherical sensor data on the surface mean plane. Each row illustrates the results obtained with a chosen strategy. Very similar results are obtained for L_1 with Heitz's approach and ours when no height constraint is applied (2^{nd} and 3^{rd} row). However, the former one produces uniform values for L_{2+} when ours provide an highlights in case of an incident angle equal to 0. The same phenomenon can be observed with V-cavities, that exhibit a higher intensity and for all incident angles. Note that the use of V-cavities tends to produce a BSDF which is very different from the results obtained using the uncorrelated assumption (which is physically much more plausible). Height limits and macro structure constraints have been applied to constrain the surface shape, for the same GGX distribution configuration. As is shown in lines 4-6 in Figure 8, L_{2+} values obtained with continuous surfaces are never close to the results obtained by Heitz's approach, showing how the micro-geometry orgnaization impacts the BSDF shape and so the material appearance).

C. Case study and analysis

To study at which slope intensity multiple scattering become prohiminent, we also use an inverse shifted heaviside step function as a normal distribution. Depending on an angle θ_c that represents the slope limit of microfacets, surfaces are generated (Figure 9). For two incident angles and one slice plane, the resulting BDRF for each surface height-map is illustrated in Figure 10. These results highlight several interesting remarks. As expected for $\theta_i = 0$, the multi-bounce L_{2+} coefficient is close to zero when micro-facet slope angle θ_c is always under $\frac{\pi}{4}$. Moreover with this configuration, L_1 is close to constant for θ_o from $-2\theta_c$ to $2\theta_c$ that corresponds to the maximum mirror angle. For different θ_i angles, L_{2+} values can be modelled by a single lobe: Thinner with a significant value towards the mirror angle when θ_c is under $\frac{3\pi}{16}$ and, larger with back-scattering reflections such as L_1 values when θ_c is over $\frac{\pi}{4}$. For lower values of θ_c from $\frac{\pi}{8}$ to $\frac{\pi}{4}$ and for $\theta_i = 0$, L_{2+} values define a two lobe function that becomes a single one. Figure 11 shows this phenomenon for lower variations of θ_c. For more grazing incident angles θ_i, the L_{2+} lobe is firstly centered to the mirror angle and it slowly shifts to produce back-scattering effects.

In the next experiment, the height level of the generated

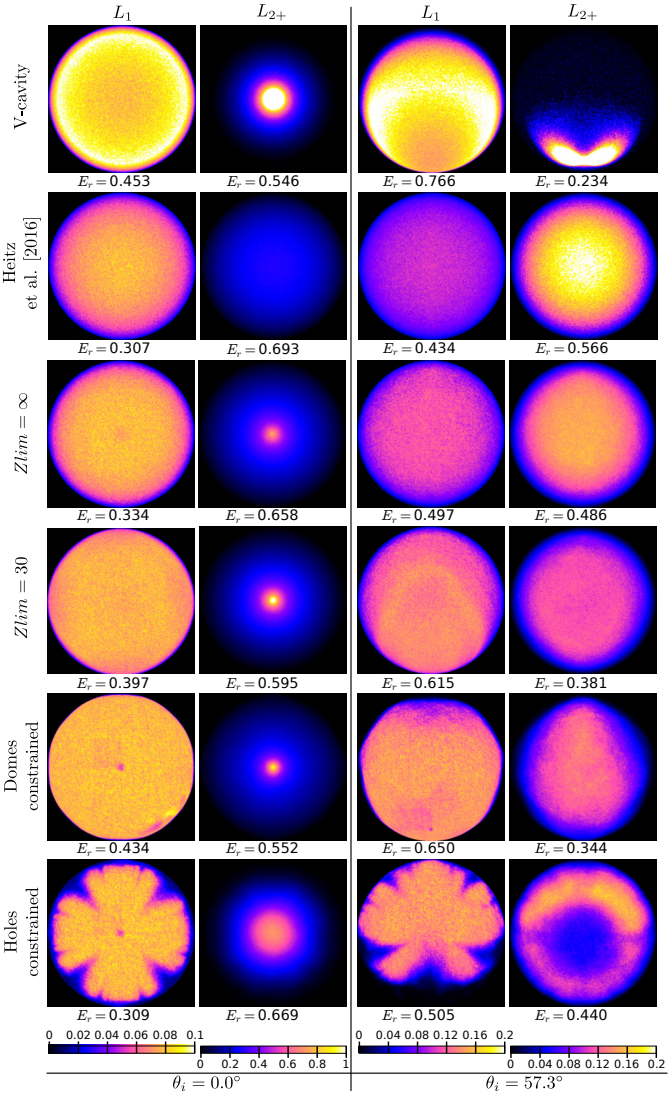

Fig. 8. Comparisons between different strategies for numerical BSDF calculation from GGX distribution with $\sigma = 1.0$. The two first rows correspond to the state of the art and the others to our method with various constraints.

height-maps is constrained, with $\theta_c = \frac{\pi}{2}$, corresponding to GGX with $\sigma = 1.0$ (third and fourth row of the figure 8 and figure 12). The auto-correlation function shows that height-maps do not contain any macro structure. Counterintuitively, L_1 is more diffuse in the case of a higher height limitation, for all incident angles (figure 13), in contrast to the L_{2+} coefficient that is thinner when θ_i equal to zero and lower than others for more grazing incident angle, as might be anticipated. Because all these height-maps do not contain any macro structure, the resulting BSDFs are fully isotropic. Rather, a macro structure constraint could strongly modified the BSDF shape. The three last rows of the figure 8 illustrate this phenomenon, for a same NDF (i.e. $\theta_c = \frac{\pi}{2}$), the holes constrained height-map produce a structured BSDF shape when domes or height limit constraints do not really modify the BSDF shape compared to unconstrained height-map generation. Finally, a visual comparison of these different results is shown in figure 14 with physically-based rendering using a path tracing method. The two state-of-the-art methods produce very different visual results. V-cavities provide mirror effects

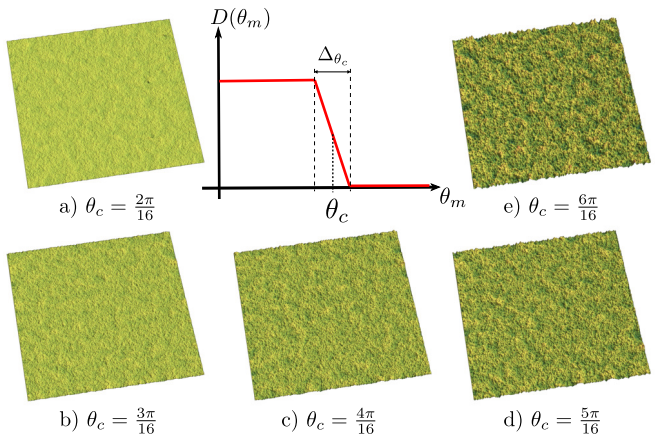

Fig. 9. Generated height-maps from an inverse shifted Heaviside step function with different value of θ_c, with $\Delta_{\theta_c} = \frac{\pi}{200}$

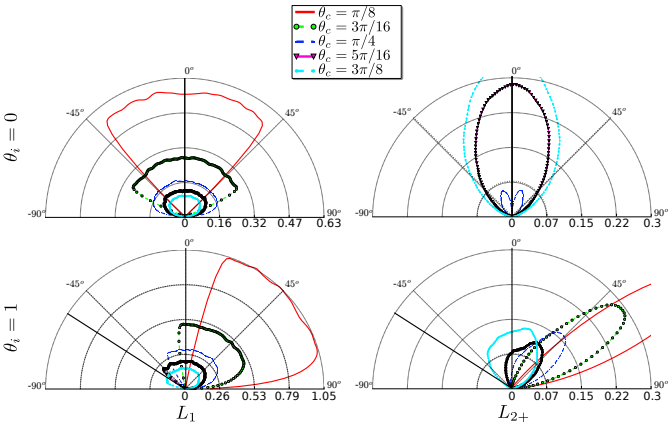

Fig. 10. BSDF results obtained from the surfaces illustrated in figure 9.

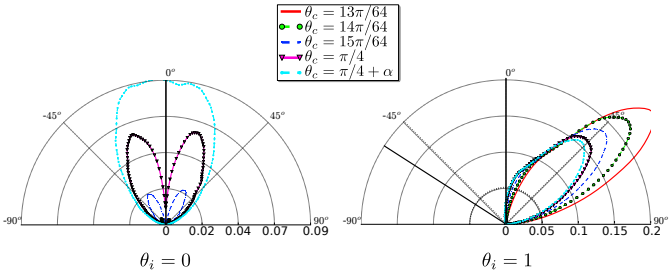

Fig. 11. L_{2+} BSDF results for low variations of θ_c around $\frac{\pi}{4}$.

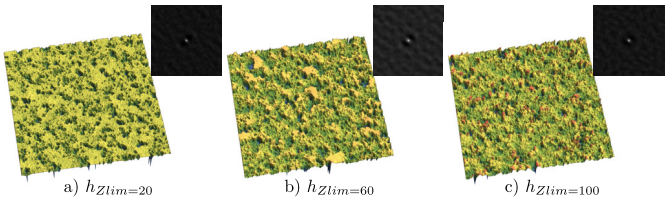

Fig. 12. Height-maps obtained form the GGX distribution with $\sigma = 1.0$ and a constraint of height limit. For each height-map, the inset shows the autocorrelation function.

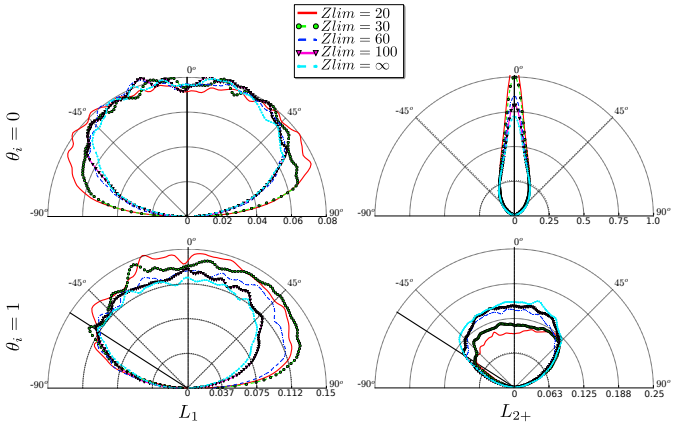

Fig. 13. BSDF results form surfaces shown in figure 12.

when Heitz's results are much closer to the expected aspects. Our method with height limitation is also close to this latter. However, different shiny effects can be also observed. More importantly, our generated height-maps with macro-geometric constraint produces very interesting results, with anisotropy despite an isotropic NDF.

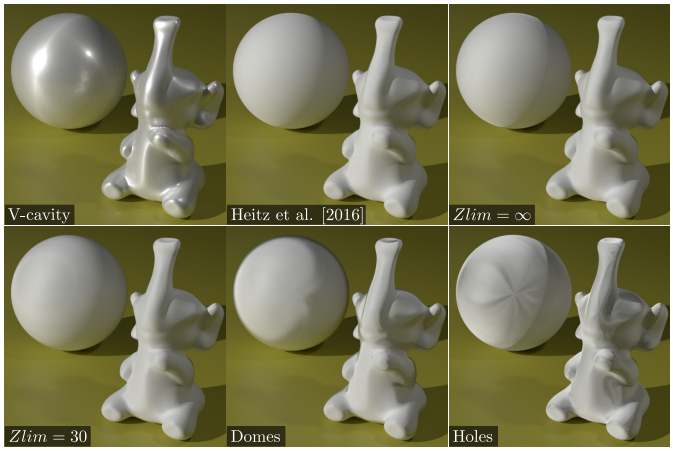

Fig. 14. Images rendered with numerical lighting simulation using BSDF from Figure 8

This phenomenon is confirmed by the BSDF as shown in figure 15 with GGX distribution with $\sigma = 1.0$ for both L_1, L_{2+} and two values of φ_i. Figure 16 illustrates the NDF of the "Domes" and "Holes" surface for various values of φ_i. Despite an isotropic NDF, this result demonstrates that the BSDF of a surface depends on different levels of microfacet geometry.

In the last experiment illustrated in this paper, hand made distribution based on an anisotropic cardinal sinus function is used to evaluate the possibilities offered by our framework. Figure 17 shows the obtained BSDF from this normal distribution whitout any constraint during surface construction. It is a well-known fact that a specific NDF has a significant impact on the appereance and this final result shows this phenomenon.

5. CONCLUSION

This paper presents a complete framework for numerically predicting the material appearance of rough microgeometries. Our approach relies on the construction of a realistic height-map

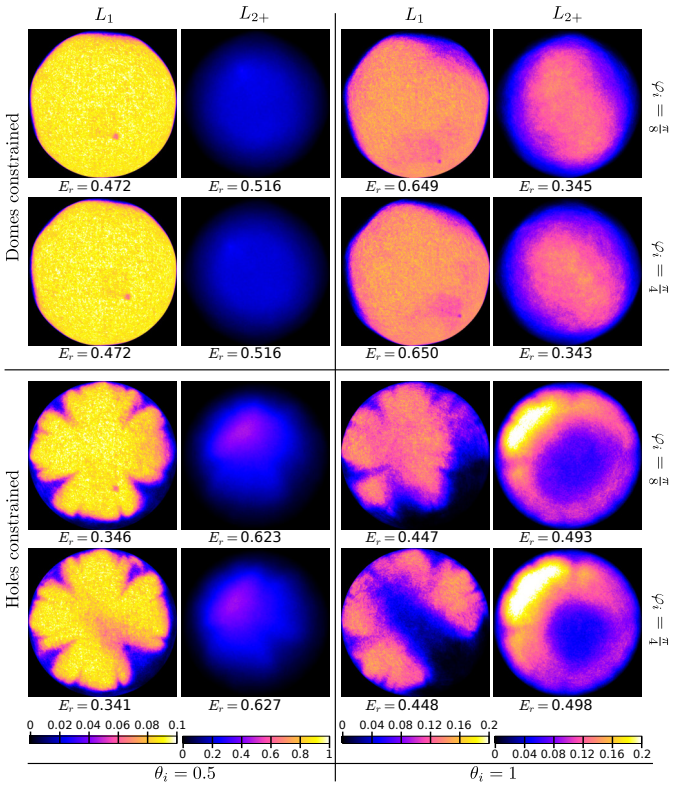

Fig. 15. Numerical BSDF calculation from GGX distribution with $\sigma = 1.0$ and two different values of φ_i for generated height-map with "Domes" or "Holes" initial constraint.

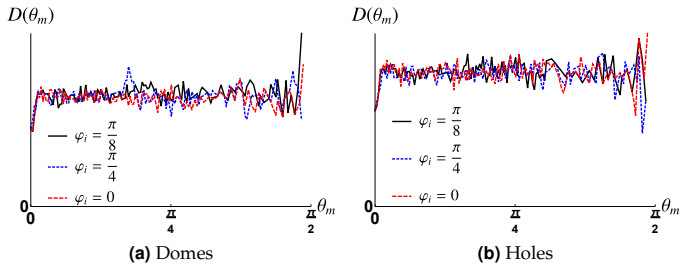

Fig. 16. Normal distribution of "Domes" and "Holes" height-map according to θ_m, for several values of φ_i.

with controlled geometric properties, for taking into account multi-bounces of light reflections. The proposed method is compared to the state of the art, with (i) the V-Cavity assumption and (ii) the fully probabilistic approach of Heitz [19] that does not relie on any practical microgeometry. As illustrated in our results, the appearance of a rough surface depends on both the normal distribution function and the macro-geometry structure (i.e. the height distribution function or geometric structure). The key feature of our framework is the management of various parameters for controlling macro- and micro-geometry, that influence the final material appearance. It is an essential step to create new BSDF models that better take account of the surface structure diversities. In the context of 3D printing, such a control on the microgeometry is mandatory in order to manage the final appearance, as shown in [1]. Thus, a natural extension of our method is to make use of the constraints due to 3D printers to

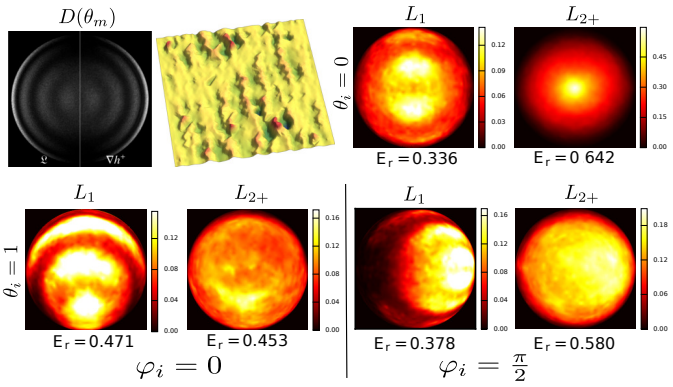

Fig. 17. A hand made anisotropic distribution: The top-left image compares the input NDF ($\mathfrak{L}$) with the resulting NDF (∇h^+), the second image corresponds to the surface generated by our process. The other images show the BSDF captured by our virtual goniophotometer.

manage side effects and control for instance new visual patterns.

Disclosures. The authors declare no conflicts of interest.

REFERENCES

1. A. Luongo, V. Falster, M. B. Doest, M. M. Ribo, E. R. Eiriksson, D. B. Pedersen, and J. R. Frisvad, "Microstructure control in 3d printing with digital light processing," Comput. Graph. Forum **n/a** (2019).
2. M. Ribardière, B. Bringier, L. Simonot, and D. Meneveaux, "Microfacet bsdfs generated from ndfs and explicit microgeometry," ACM Trans. Graph. **38**, 143:1–143:15 (2019).
3. E. Heitz, "Generating procedural beckmann surfaces," Tech. rep. (2015). Https://eheitzresearch.wordpress.com/research/.
4. E. Heitz, J. Hanika, E. d'Eon, and C. Dachsbacher, "Multiple-scattering microfacet bsdfs with the smith model," ACM Transactions On Graph. SIGGRAPH Asia proceedings **35** (2016).
5. K. E. Torrance and E. M. Sparrow, "Theory for off-specular reflection from roughened surfaces," J. Opt. Soc. Am. **57** (1967).
6. R. L. Cook and K. E. Torrance, "A reflectance model for computer graphics," in *ACM SIGGRAPH proceedings,* (1982).
7. C. Bourlier, G. Berginc, and J. Saillard, "One- and two-dimensional shadowing functions for any height and slope stationary uncorrelated surface in the monostatic and bistatic configurations," IEEE Transactions on Antennas Propag. **50** (2002).
8. M. Oren and S. K. Nayar, "Generalization of lambert's reflectance model," in *ACM SIGGRAPH proceedings,* (1994).
9. M. Ashikhmin, S. Premoze, and P. Shirley, "A microfacet-based BRDF generator," in *Proceedings of the 27th Annual Conference on Computer Graphics and Interactive Techniques, SIGGRAPH 2000, New Orleans, LA, USA, July 23-28, 2000,* (ACM, 2000), pp. 65–74.
10. C. Kelemen and L. Szirmay-Kalos, "A Microfacet Based Coupled Specular-Matte BRDF Model with Importance Sampling," in *Eurographics 2001 - Short Presentations,* (Eurographics Association, 2001).
11. B. Walter, S. R. Marschner, H. Li, and K. E. Torrance, "Microfacet models for refraction through rough surfaces," in *Computer Graphics Forum, EGSR proceedings,* (2007).
12. M. M. Bagher, C. Soler, and N. Holzschuch, "Accurate fitting of measured reflectances using a shifted gamma micro-facet distribution," Comput. Graph. Forum **31** (2012).
13. J. Dupuy, E. Heitz, J. Iehl, P. Poulin, F. Neyret, and V. Ostromoukhov, "Linear efficient antialiased displacement and reflectance mapping," ACM Trans. Graph. **32**, 211:1–211:11 (2013).
14. M. Ribardière, B. Bringier, D. Meneveaux, and L. Simonot, "STD: Student's t-Distribution of Slopes for Microfacet Based BSDFs," Comput. Graph. Forum (2017).

15. E. Heitz, "Understanding the masking-shadowing function in microfacet-based brdfs," J. Comput. Graph. Tech. **3** (2014).
16. B. Smith, "Geometrical shadowing of a random rough surface," IEEE Transactions on Antennas Propag. **15**, 668–671 (1967).
17. V. Ross, . Dion, and G. Potvin, "Detailed analytical approach to the gaussian surface bidirectional reflectance distribution function specular component applied to the sea surface," J. Opt. Soc. Am. A **22** (2005).
18. E. Heitz, C. Bourlier, and N. Pinel, "Correlation effect between transmitter and receiver azimuthal directions on the illumination function from a random rough surface," Waves in Random and Complex Media **23** (2013).
19. E. Heitz, J. Hanika, E. d'Eon, and C. Dachsbacher, "Multiple-scattering microfacet bsdfs with the smith model," ACM Trans. Graph. **35**, 58:1–58:14 (2016).
20. P. Beckmann and A. Spizzichino, *The scattering of electromagnetic waves from rough surfaces* (Pergamon Press, 1963).
21. C. Kulla and A. Conty, "Physically based shading in theory and practice - revisiting physically based shading at imageworks," in *ACM SIGGRAPH 2017 Courses,* (2017).
22. E. Turquin, "Practical multiple scattering compensation for microfacet models," Tech. rep. (2019).
23. J. H. Lee, A. Jarabo, D. S. Jeon, D. Gutierrez, and M. H. Kim, "Practical multiple scattering for rough surfaces," ACM Trans. Graph. **37**, 275:1–275:12 (2018).
24. F. Xie and P. Hanrahan, "Multiple scattering from distributions of specular v-grooves," ACM Trans. Graph. **37**, 276:1–276:14 (2018).
25. D. Saint-Pierre, P. Chavel, L. Simonot, and M. Hébert, "Angular reflectance model for ridged specular surfaces, with comprehensive calculation of inter-reflections and polarization," J. Opt. Soc. Am. A **36**, C51–C61 (2019).
26. T. H. Naylor, J. L. Balintfy, D. S. Burdick, and K. Chu, *Computer Simulation Techniques* (Wiley, 1966).
27. E. I. Thorsos, "The validity of the kirchhoff approximation for rough surface scattering using a gaussian roughness spectrum," J. Acoust. Soc. Am. **83**, 78–92 (1988).
28. J. S. Gondek, G. W. Meyer, and J. G. Newman, "Wavelength dependent reflectance functions," in *Proceedings of the 21st Annual Conference on Computer Graphics and Interactive Techniques,* (ACM, New York, NY, USA, 1994), SIGGRAPH '94, pp. 213–220.
29. A. Luongo, V. Falster, M. B. Doest, D. Li, F. Regi, Y. Zhang, G. Tosello, J. Nielsen, H. Aanæs, and J. R. Frisvad, "Modeling the anisotropic reflectance of a surface with microstructure engineered to obtain visible contrast after rotation," in *ICCV 2017 Workshops,* (2017), pp. 159–165.
30. T. Pereira, C. L. A. P. Leme, S. Marschner, and S. Rusinkiewicz, "Printing anisotropic appearance with magnetic flakes," ACM Trans. Graph. **36**, 123:1–123:10 (2017).
31. T. Weyrich, P. Peers, W. Matusik, and S. Rusinkiewicz, "Fabricating microgeometry for custom surface reflectance," ACM Trans. Graph. **28**, 32:1–32:6 (2009).
32. M. Papas, W. Jarosz, W. Jakob, S. Rusinkiewicz, W. Matusik, and T. Weyrich, "Goal-based caustics," Comput. Graph. Forum (Proc. Eurographics) **30** (2011).
33. Y. Schwartzburg, R. Testuz, A. Tagliasacchi, and M. Pauly, "High-contrast computational caustic design," ACM Trans. Graph. **33**, 74:1–74:11 (2014).
34. B. K. P. Horn, "Shape from shading: a method for obtaining the shape of a smooth opaque object from one view," Tech. rep., Cambridge, MA, USA (1970).
35. W. Xie, Y. Zhang, C. C. L. Wang, and R. C. k. Chung, "Surface-from-gradients: An approach based on discrete geometry processing," in *2014 IEEE Conference on Computer Vision and Pattern Recognition, CVPR 2014, Columbus, OH, USA, June 23-28, 2014,* (2014), pp. 2203–2210.
36. A. Agrawal, R. Raskar, and R. Chellappa, "What is the range of surface reconstructions from a gradient field?" in *Proceedings of the 9th European Conference on Computer Vision - Volume Part I,* (Springer-Verlag, Berlin, Heidelberg, 2006), ECCV'06, pp. 578–591.
37. R. T. Frankot and R. Chellappa, "A method for enforcing integrability in shape from shading algorithms," IEEE Trans. Pattern Anal. Mach. Intell. **10**, 439–451 (1988).
38. B. Beckers and P. Beckers, "A general rule for disk and hemisphere partition into equal-area cells," Comput. Geom. **45**, 275 – 283 (2012).
39. B. Cabral, N. Max, and R. Springmeyer, "Bidirectional reflection functions from surface bump maps," SIGGRAPH Comput. Graph. **21**, 273–281 (1987).
40. S. H. Westin, J. R. Arvo, and K. E. Torrance, "Predicting reflectance functions from complex surfaces," SIGGRAPH Comput. Graph. **26**, 255–264 (1992).
41. O. Moreau and T. R. Leroux, "Fast and accurate measurement of liquid crystal tilt bias angle with the ELDIM EZContrast system," in *Polarization and Color Techniques in Industrial Inspection,* vol. 3826 E. A. Marszalec and E. Trucco, eds., International Society for Optics and Photonics (SPIE, 1999), pp. 236 – 241.
42. G. Obein, O. Shiraz, and G. Ged, "Evaluation of the shape of the specular peak for high glossy surfaces," Proc. SPIE - The Int. Soc. for Opt. Eng. **9018** (2014).